

Neutron resonance parameters of $^{68}\text{Zn} + n$ and statistical distributions of level spacings and widths

J. B. Garg and V. K. Tikku

State University of New York, Albany, New York 12222

J. A. Harvey, J. Halperin, and R. L. Macklin

Oak Ridge National Laboratory, Oak Ridge, Tennessee 37830

(Received 2 November 1981)

Discrete values of the parameters (E_0 , $g\Gamma_n$, J^π , Γ_γ , etc.) of the resonances in the reaction $^{68}\text{Zn} + n$ have been determined from total cross section measurements from a few keV to 380 keV with a nominal resolution of 0.07 ns/m for the highest energy and from capture cross section measurements up to 130 keV using the pulsed neutron time-of-flight technique with a neutron burst width of 5 ns. The cross section data were analyzed to determine the parameters of the resonances using R -matrix multilevel codes. These results have provided values of average quantities as follows: $S_0 = (2.01 \pm 0.34)$, $S_1 = (0.56 \pm 0.05)$, $S_2 = (0.2 \pm 0.1)$ in units of 10^{-4} , $D_0 = (5.56 \pm 0.43)$ keV and $D_1 = (1.63 \pm 0.14)$ keV. From these measurements we have also determined the following average radiation widths: $(\bar{\Gamma}_\gamma)_{l=0} = (302 \pm 60)$ meV and $(\bar{\Gamma}_\gamma)_{l=1} = (157 \pm 7)$ meV. The investigation of the statistical properties of neutron reduced widths and level spacings showed excellent agreement of the data with the Porter-Thomas distribution for s - and p -wave neutron widths and with the Dyson-Mehta Δ_3 statistic and the Wigner distribution for the s -wave level spacing distribution. In addition, a correlation coefficient of $\rho = 0.50 \pm 0.10$ between Γ_n^0 and Γ_γ has been observed for s -wave resonances. The value of $\langle \sigma_{n\gamma} \rangle$ at (30 ± 10) keV is 19.2 mb.

[NUCLEAR REACTIONS $^{68}\text{Zn}(n, n)$, $^{68}\text{Zn}(n, \gamma)$, $E = \text{few keV to } 380, 130 \text{ keV}$, respectively. Measured total and capture cross sections versus neutron energy, deduced resonance parameters, E_0 , J^π , $g\Gamma_n$, Γ_γ , S_0 , S_1 , S_2 , D_0 , D_1 .]

I. INTRODUCTION

The investigation of the properties of parameters of highly complex states in nuclei has provided interesting information about the ordering of these levels in agreement with the random matrix model of Wigner.¹ Similarly, the distribution of s -wave neutron reduced widths was found to be in general agreement with the Porter-Thomas distribution.² Later theoretical work by Dyson and Mehta³ predicted a long range correlation in the eigenvalues of a real symmetric Hamiltonian, as in a crystalline structure. These predictions were successfully tested in a series of papers reported by groups at Columbia University from high-resolution measurements of the neutron total cross sections of rare-earth nuclei; in particular, the measurements⁴ on the isotope ^{166}Er gave excellent agreement with the predicted value of the Δ_3 statistic of Dyson and Mehta.³

We have recently investigated these properties with high resolution measurements of the neutron total cross section of ^{64}Zn and ^{66}Zn and pointed out the success of the Dyson-Mehta model.³ In particular, we noted that in view of the sensitivity of this Δ_3 statistic to the precise locations of missed or spurious levels, that it was essential to ascertain the J^π assignment of each resonance to verify the validity of this statistic. This task was accomplished with a high degree of confidence in our

measurements^{5,6} on the basis of the observation of shapes of resonances, which are asymmetric for s -wave resonances and essentially symmetric for $l > 0$ resonances. The assignments for very small resonances were made from a shape analysis of resonances using the R -matrix formalism of Wigner and Eisenbud.⁷

In this paper, we present results of resonance parameters on another even-even nucleus ($^{68}\text{Zn} + n$). The previous information⁸ on the resonance parameters of this nucleus is very sparse and the present results fill the gap in the data for this nuclide.

The measurement of the neutron total cross section of this nuclide has been supplemented by the measurement of neutron capture cross sections. In view of the greater sensitivity of the capture measurements for resonances with very small neutron widths, a large number of very narrow resonances missed in the transmission data was observed in the capture data. A combination of these sets of data provides almost a complete level sequence of p -wave resonances and a partial sequence of d -wave resonances. In addition, the capture data provided information about the total radiation widths of many of the resonances and gave average capture cross section values as a function of neutron energy which are useful quantities for reactor shielding and for the understanding of stellar nucleosynthesis of the elements.⁹

II. EXPERIMENTAL PROCEDURE

The cross section measurements were performed with the high resolution neutron time-of-flight facility at the Oak Ridge National Laboratory whose essential features for such measurements have been previously described.¹⁰ For the total cross section measurements, we used a flight path of 78.203 m and time windows which varied in steps of a factor of 2 from a minimum value of 1 ns for the energy region above 30 keV to 32 ns below 50 eV. The electron linear accelerator was operated at a power of 10 kW with a burst width of 5 ns at a repetition rate of 800 Hz. The capture cross section measurements were performed at a flight path of 40 m with similar operating conditions of the linear accelerator, but with 1, 2, 4 and 8 ns time windows. For the transmission measurements, two samples of ZnO enriched to 99.28% in mass 68 with inverse thicknesses of $1/n = 10.44$ and 59.23 b/a for the ^{68}Zn isotope were used. The oxide powder sample was pressed inside a polyethylene tube of 2.54 cm diameter. Measurements were also made with natural zinc samples of inverse thicknesses $1/n =$

TABLE I. Atomic percent abundance of other zinc isotopes in the sample enriched in ^{68}Zn .

Mass number	64	66	67	68	70
% abundance	0.26	0.27	0.19	99.28	<0.1

75 and 300 b/a for energies below ~ 1 keV. For the capture measurements, the sample was also of ZnO of similar enrichment as given in Table I, but pressed to a thickness of 0.6 cm, in the shape of a disc with a radius of 1.3 cm. The sample weighed 6.94 g.

The detector used for the total cross section measurements for neutron energies above 30 keV was an NE-110 fast scintillator mounted on a 127 mm diameter RCA 4522 photomultiplier tube. A ^6Li glass scintillator 1.3 cm thick was used below 30 keV. The total duration for these measurements was about one week of accelerator running time. The analysis of the data was carried

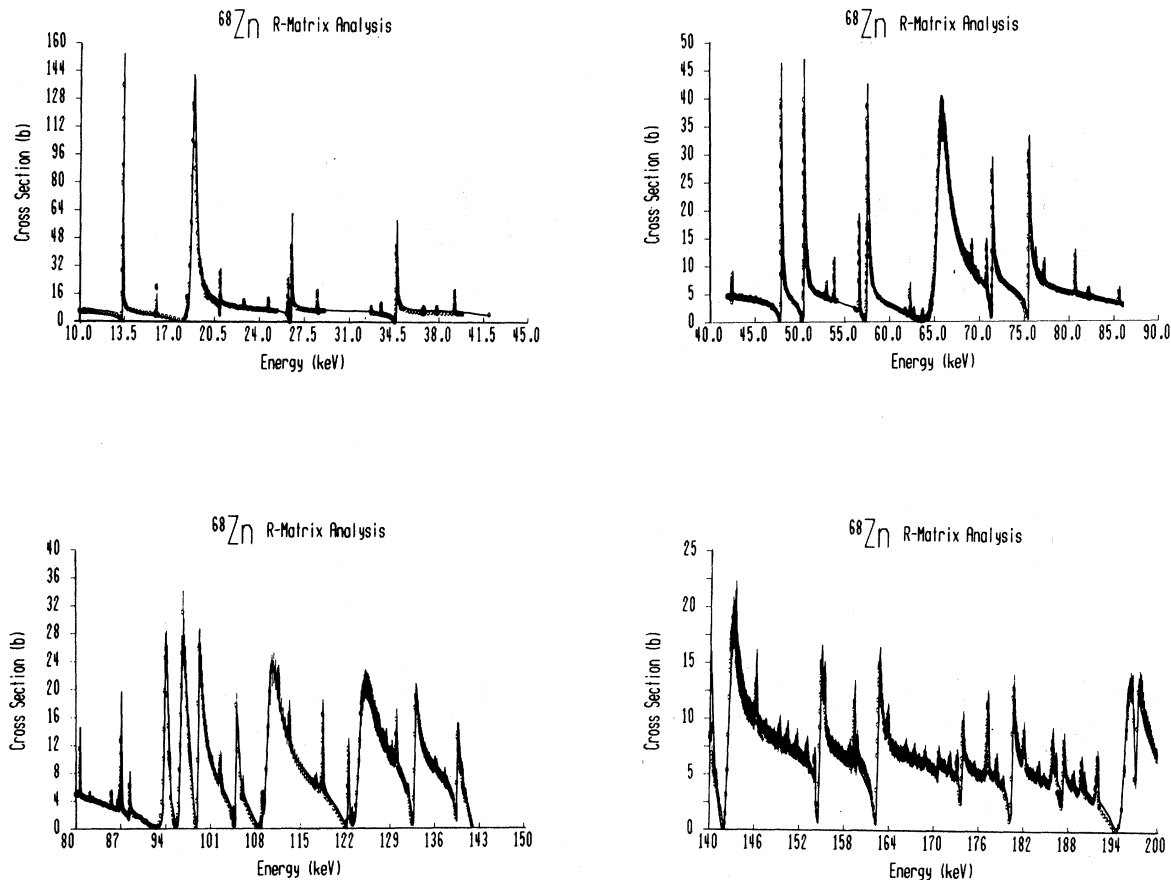


FIG. 1. The total cross section data for ^{68}Zn nucleus in the neutron energy range from 10 to 200 keV. The solid curves are the theoretical cross section values obtained from an R-matrix multilevel analysis. The solid curves are slightly off center due to the misalignment of the plotting machine.

out over a period of about one year.

For the capture measurements, the sample was placed between a pair of total energy γ -ray detectors. The neutron beam was narrowly collimated to impinge only on the capture sample and to avoid hitting the detectors. The details of the experimental arrangement have been given in previous publications.¹¹ These data were taken over a period of one week.

III. DATA MANIPULATION

The total cross section was determined from the transmission of the neutron beam through the sample. Since the measurements of neutron intensities with and without the sample in position were made cyclically for different time intervals, the neutron counts had to be normalized to the same neutron monitor counts and had to be corrected for the dead time of the time digitizer. Various backgrounds, which were functions of the time of flight and the accelerator operating conditions were carefully evaluated in the manner discussed in

an earlier publication.¹² After correcting for the contribution of the oxygen in the sample, the total cross section of the ^{68}Zn as a function of neutron energy was obtained. The results are shown in Figs. 1 and 2 in the energy intervals 10 to 200 keV and 200 to 380 keV, respectively, along with the theoretical fits. The solid curves are the R-matrix multilevel theoretical fits for a nuclear radius of 5.6 from the computer code MULTI.¹³ The fitting was done on a UNIVAC 1110 computer at the State University of New York at Albany. The fit to the experimental data is very good except for some isolated intervals, such as between 257 and 263 keV.

A similar manipulation of raw data for the capture cross section measurements allowed us to obtain curves of capture cross section vs energy, which are shown in Figs. 3 and 4 in the energy intervals 2.5 to 60 keV and 60 to 160 keV neutron energy, respectively. The solid curves are only eye guides, not the fits as obtained from the LSFIT program.¹⁴ Values of the parameters for s-wave resonances obtained from these analyses are given in Tables III and IV.

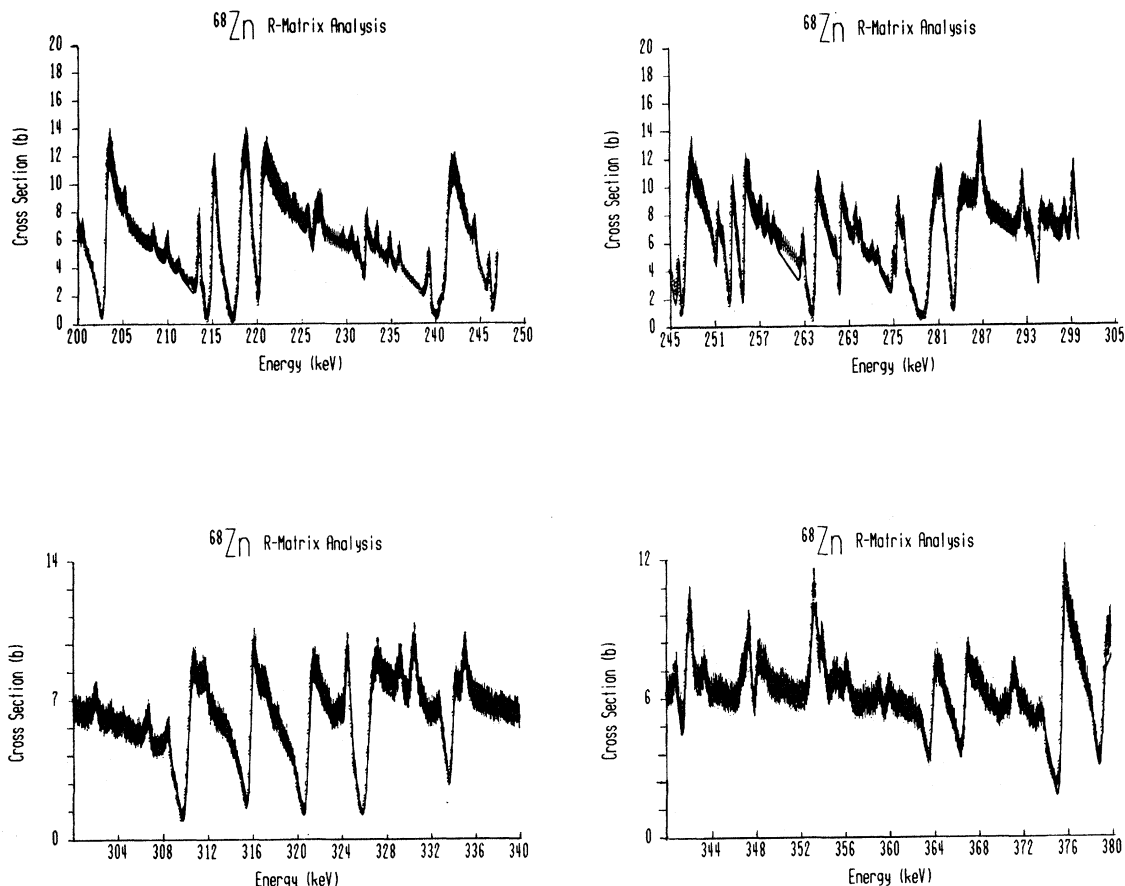


FIG. 2. The neutron total cross section data for ^{68}Zn from 200 to 380 keV energy interval. The solid curves are the theoretical R-matrix fit. The same comments as in Fig. 1 apply.

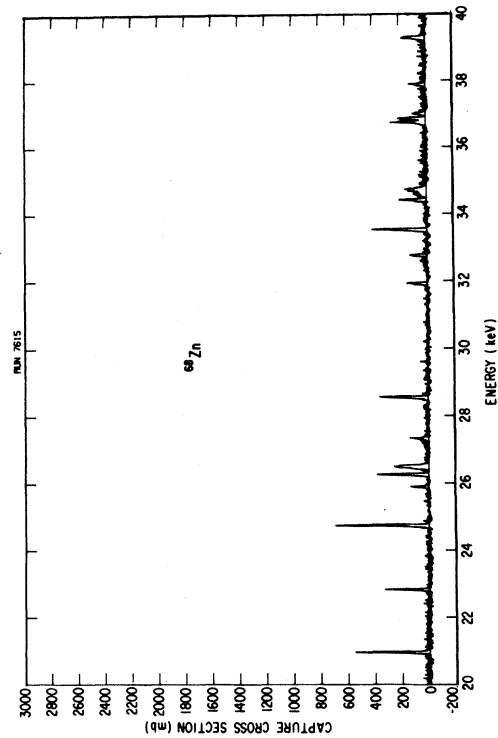
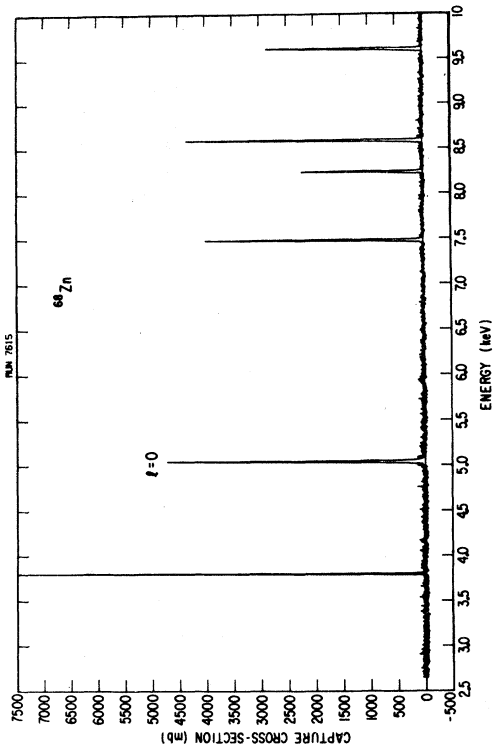
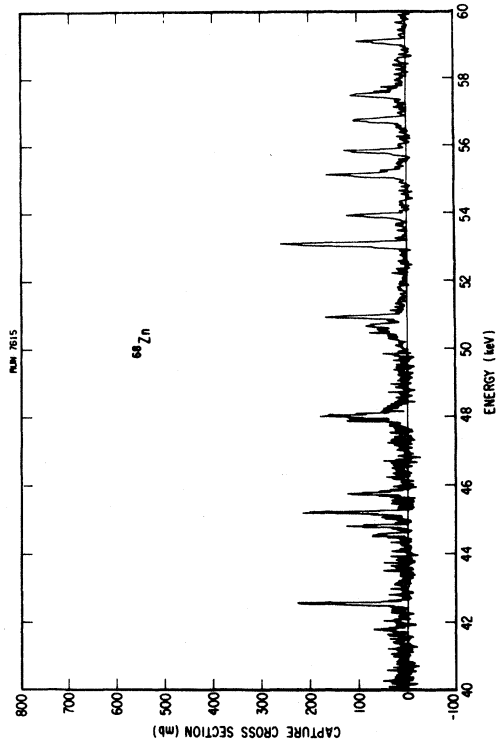
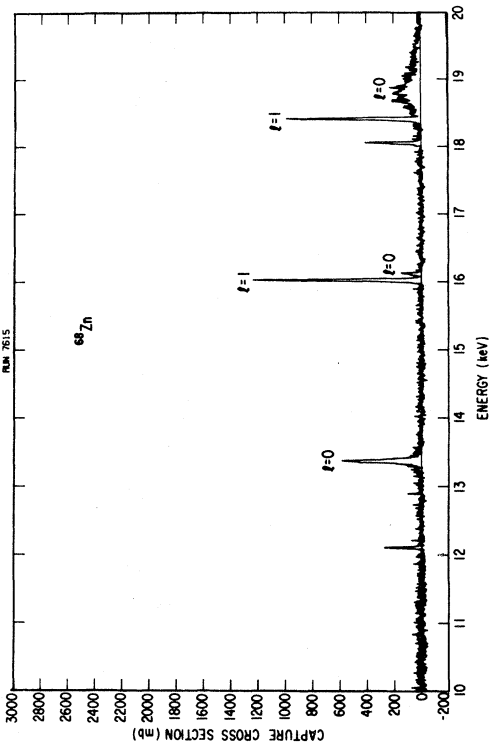


FIG. 3. The neutron capture cross section data for a thin oxide sample of ^{68}Zn nucleus in the neutron energy range of 2.5 to 60 keV. The solid curves are drawn through the data points.

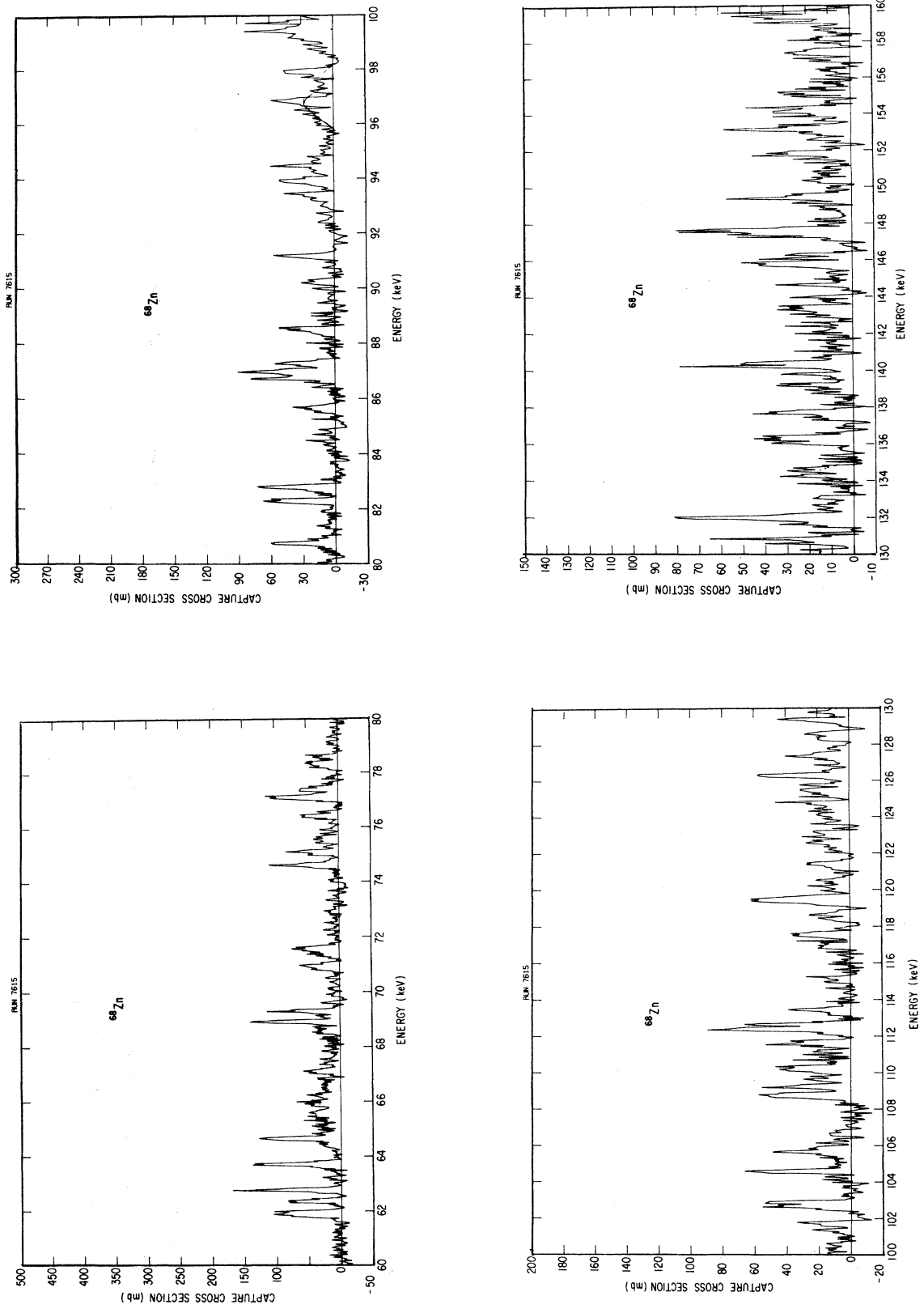


FIG. 4. The neutron capture cross section for ^{68}Zn from 60 to 160 keV.

TABLE II. Minimum value of $g\Gamma_n$ (eV) for which a clear asymmetry in the resonance shape can be observed at a given energy with the present energy resolution and ^{68}Zn sample thickness used. Column 4 gives the ratio of corresponding Γ_n^0 to the average value, which has been determined from this experiment up to 300 keV. Column 5 gives the percentage loss of levels according to the Porter-Thomas distribution in each energy interval due to the sensitivity of measurement. Column 6 gives the number of observed levels and column 7 gives the estimated number of levels missed in each 100 keV energy interval.

E_0 (keV)	Γ_n (eV) $g=1$ for s wave	Γ_n^0 (eV)	$x = \frac{\Gamma_n^0}{\langle \Gamma_n^0 \rangle}$ ($\langle \Gamma_n^0 \rangle = 1.2$ eV)	% Loss of levels from $x=0$ to x	No. of observed levels	Total loss of levels
0-20	0.3	2×10^{-3}	1.7×10^{-3}	3.2	4	1.0
20-40	0.5	2.5×10^{-3}	2.1×10^{-3}	3.5	3	
40-80	2.0	7×10^{-3}	5.8×10^{-3}	6.0	7	
80-100	2.5	8×10^{-3}	6.6×10^{-3}	6.3	4	
100-170	4.0	1.0×10^{-2}	8.3×10^{-3}	6.9	11	1.3
170-200	5.0	1.2×10^{-2}	1.0×10^{-2}	7.6	7	
200-250	8	1.6×10^{-2}	1.3×10^{-2}	8.5	9	1.7
250-300	10	1.8×10^{-2}	1.5×10^{-2}	9.2	11	

IV. DISCUSSION OF RESULTS

A. Uncertainties in resonance parameters

A discussion of the associated uncertainties in the resonance energies and $g\Gamma_n$ values has been given previously⁶ and, hence, these will not be discussed again here.

B. Neutron reduced width distribution for s-wave resonances

A plot of the square roots of neutron reduced widths for all the observed s-wave resonances up to $E_n \sim 300$ keV is shown in Fig. 5. The only criterion for making the parity assignment of resonances has been

TABLE III. The parameters of s-wave resonances obtained from the total and capture cross section measurements. The values for E_0 and Γ_n were obtained from the R-matrix analysis of transmission data. The capture area A and its uncertainty are obtained from LSFIT analysis of capture data. The last two columns give values of Γ_γ and its uncertainty after subtraction of $k\Gamma_n$.

E_0 (eV)	ΔE_0 (eV)	A = $\Gamma_n (\Gamma_\gamma + k\Gamma_n) / \Gamma$ (meV)	Γ_n (eV)	$\Delta \Gamma_n$ (eV)	k (10^{-3})	Γ_γ (meV)	$\Delta \Gamma_\gamma$ (meV)
516.4	0.2		8.5	0.5			
5040	2	75.6 ± 2.8	5.5	0.6	0.69	73	3
13373	5	195.1 ± 5.4	28	2.0	0.43	185	6
18828	6	520.1 ± 15.9	320	10.	0.37	403	28
20950	6	146.1 ± 4.0	3.5	0.5	0.38	152	5
26506	10	242.1 ± 2.1	25	1.	0.55	231	5
34691	10	232.0 ± 14.0	52	2.	0.58	203	17
42540	15	219.4 ± 12.2	2.	0.5	0.35	233	13
47998	15	250.8 ± 46.1	97.	3.	0.39	214	50
50544	15	210.6 ± 23.4	150.	4.	0.44	145	29
57603	15	210.6 ± 36.0	162.	3.	0.31	161	41
65660	15	1583.3 ± 104.3	1180.	60.	0.25	1290	135
71513	20	358.8 ± 36.9	77.	3.	0.24	341	39
75598	20	292.2 ± 30.3	165.	7.	0.24	253	33
88489	20	190.3 ± 57.0	12.	2.	0.33	189	58
93875	20	348.0 ± 127.0	622.	8.	0.40	99	35
96625	20	496.0 ± 147.0	780.	20.	0.40	184	80
99450	20	955.0 ± 159.0	560.	10.	0.39	737	145
105110	25	413.3 ± 65.1	205.	20.	0.37	338	56
110400	25	1408.0 ± 223.0	1775.	25.	0.34	806	175
117500	25	292.2 ± 80.0	4.	2.	0.32	308	85
122570	25	167.7 ± 75.4	110.	5.	0.35	129	67
124600	25	740.0 ± 265.9	2100.	50.	0.33	44	20

TABLE IV. The s-wave resonance parameters (in eV) obtained from the R-matrix analysis of total cross section data from 130 keV to 380 keV.

E_O	ΔE_O	Γ_n	$\Delta \Gamma_n$	E_O	ΔE_O	Γ_n	$\Delta \Gamma_n$
133000	25	500	25	253210	50	254	12
139600	25	155	15	254960	50	600	50
142700	30	1350	65	264520	50	740	50
154760	30	260	20	267865	50	330	25
159790	30	10	2	270000	50	80	10
162520	35	295	15	275500	50	350	25
170625	35	11	2	279960	55	2060	100
173820	35	63	6	283495	55	1225	60
180520	40	200	15	291800	55	80	8
185970	40	30	6	294560	55	217	20
187380	40	45	8	310255	55	760	75
195700	40	1500	75	315738	55	453	45
197200	40	180	10	320920	55	736	70
203100	45	950	50	326300	60	1142	100
215060	45	620	6	333830	60	332	30
218190	45	1180	60	341500	60	134	15
220480	45	670	30	347900	60	177	20
226370	50	35	5	352800	60	260	25
230500	50	10	2	359550	60	45	10
232139	50	63	10	363630	60	175	20
241400	50	1650	80	366490	60	182	20
247200	50	1800	100	375245	60	521	50
251300	50	77	10	379000	60	431	50

the shapes of the resonances. S-wave resonances have an asymmetrical shape due to the coherent interference between the resonance and potential scattering; whereas, no detectable asymmetry is expected for $\ell > 0$ resonances below a few hundred keV. Figs. 1 and 2 clearly show many resonances which have striking asymmetrical shapes which were fitted with the R-matrix theory as s-wave resonances and provide accurate values of resonance energies and neutron widths. It is equally obvious that many broad reso-

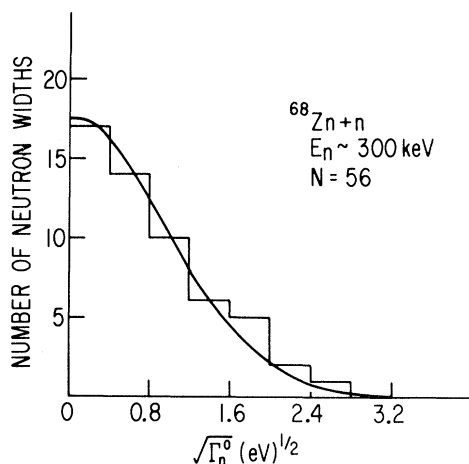


FIG. 5. Reduced neutron width amplitude distribution for s-wave resonances of $^{68}\text{Zn}+n$ observed up to 300 keV neutron energy. The curve is the Porter-Thomas distribution normalized for 56 observed resonances.

nances do not show such asymmetrical shapes and they were fitted very well assuming them to be p-wave resonances having spins of $1/2$ or $3/2$. For the very narrow resonances, there was little difference in the shape for s- and p-wave resonances and assignments were difficult. A typical case is illustrated in Fig. 6.

Examining the expanded σ_T vs E_n cross section curve in Fig. 6, we see clearly that the resonance at 170.6 keV with $\Gamma_n \sim (11 \pm 2)$ eV has a very distinct asymmetrical shape which could only be fitted as s wave; whereas, the two resonances at about 167.5 and 168.9 keV with $g\Gamma_n \sim 5$ eV could not be successfully fitted as s waves. The fit for the resonance at 168.0 keV with $g\Gamma_n \sim 2$ eV was somewhat ambiguous. We concluded from our analysis that the parity of resonances with $g\Gamma_n \geq 4$ eV at ~ 170 keV could be determined. Similar analyses over the entire range of 0-300 keV allowed us to identify the $\ell=0$ and $\ell > 0$ resonances and provided us the limiting values of $g\Gamma_n$ where a positive identification of $\ell=0$ resonances could be made from these data. These are given in Table II. Positive identifications of $\ell=0$ resonances were made if their $\Gamma_n^0 = \Gamma_n/\sqrt{E}$ (in eV) were $\geq 1.0\%$ of the mean value for $E_n \sim 200$ keV, $\sim 1.5\%$ for 300 keV and $< 1.0\%$ at energies below 200 keV as shown in Table II. This sensitivity depends upon the sample thickness and the statistical accuracy of the data.

If the distribution of reduced neutron widths follows a Porter-Thomas distribution, about 7.6% of the neutron reduced widths would be $< 1\%$ of the average reduced neutron width and about 10.5% would be $< 2\%$. These would correspond to about 4 and 6 widths, respectively, for a total of 56 s-wave widths observed in the energy interval up to 300 keV, with values of $\Gamma_n^0 < 0.012$ eV and < 0.024 eV, respectively. We observed experimentally two resonances with Γ_n^0

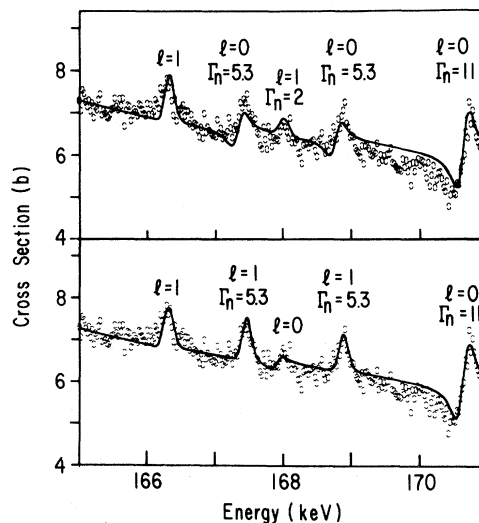


FIG. 6. Expanded σ_T vs E_n curves in the energy interval of 165 to 171 keV.

$\lesssim 0.012$ eV and six resonances with $\Gamma_n^0 \sim 0.024$ eV, indicating a deficiency of 2 of the narrowest levels and an excess of 2 widths between 0.012 and 0.024. A comparison of the experimental data on $(\Gamma_n^0)^{1/2}$ up to $E_n = 300$ keV plotted as a histogram in intervals of 0.40 eV $^{1/2}$ shows excellent agreement with the Porter-Thomas distribution except perhaps for the deficiency of one very narrow width in the first interval. An examination of Table II, however, indicates that we should have missed 4 of the narrowest resonances up to 300 keV due to the finite sensitivity of the measurements. This estimation seems to be inconsistent with our experimental observation. Monte Carlo analyses of the experimental reduced widths for the determination of the number of degrees of freedom for a chi squared distribution gave values of $\nu = 0.97^{+0.25}_{-0.18}$ and $1.1^{+0.25}_{-0.27}$ up to 250 and 300 keV, respectively. Both are in excellent agreement with the Porter-Thomas distribution which is a chi-squared distribution with one degree of freedom. A typical example of this analysis is shown in Fig. 7. The value of ν corresponds to the 50% probability value for the curve and the uncertainties represent 10% and 90% limits. In summary, the s-wave neutron reduced width distribution for the reaction $^{68}\text{Zn}+n$ is in agreement with the well established theoretical distribution of Porter-Thomas² within at most 7% of statistical uncertainty. This uncertainty could be further reduced by improving the resolution and statistics or by using a thick metallic sample in order to be able to observe the shapes of weak resonances better.

C. Distribution of reduced neutron widths for p-wave resonances

The investigation of the distribution of reduced neutron widths for resonances with $\ell > 0$ has posed serious experimental problems in the past and the assignment of parities of small resonances is often ambiguous.

We have analyzed the $\ell > 0$ observed resonances in the total as well as in the capture cross section data using the MULTI¹³ and LSFIT¹⁴ programs. The results of these analyses are given in Tables V and VI. The capture data were analyzed up to only 130 keV neutron energy since there was excessive overlapping of resonances at higher energies. The distribution compared to a Porter-Thomas distribution is shown in Fig. 8. The resonances constitute a mixed series of two level spins $J^\pi = 1/2^-$ and $3/2^-$, since few spin assignments can be obtained from these measurements. About 100 $\ell > 0$ resonances were observed up to $E_n \sim 130$ keV.

It is obvious from Fig. 8 that there is an excess of small widths [$(g\Gamma_n^1)^{1/2} < 0.2$ eV $^{1/2}$] compared to a Porter-Thomas distribution. Hence, we calculated from the expression given in an earlier publication⁶ the d-wave probabilities for all $\ell > 0$ neutron widths for assumed values of $S_1 = 0.56 \times 10^{-4}$, $S_2 = 0.2 \times 10^{-4}$, $D_1 = 1.63$ keV

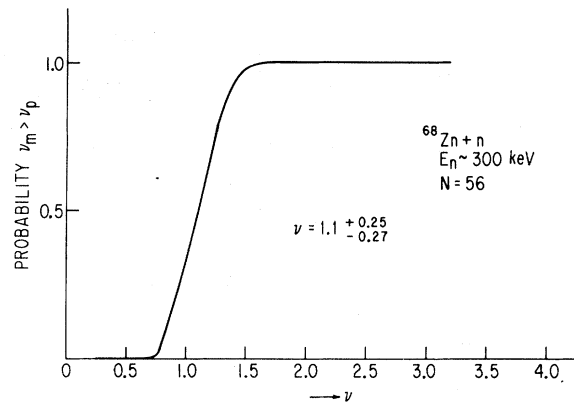


FIG. 7. Monte Carlo analysis of the distribution of s-wave neutron widths of $^{68}\text{Zn}+n$. This gives a value of $\nu = 1.10^{+0.25}_{-0.27}$ up to $E_n \sim 300$ keV. The value of ν is more significant for a comparison than the visual curve shown in Fig. 5.

and $R = 5.6$ fm. It is seen from Table V that up to $E_n \sim 130$ keV, there are about 20 resonances whose $g\Gamma_n$ were small enough to have a d-wave probability of 50% or larger. Assuming that these were d-wave resonances and normalizing the neutron width distribution of the 80 remaining resonances, we obtained much better agreement with the Porter-Thomas distribution for $(g\Gamma_n^1)^{1/2} < 0.4$ eV $^{1/2}$.

Moreover, the Monte Carlo analysis of all 100 resonances observed up to 130 keV gave a value of $\nu = 0.79^{+0.19}_{-0.19}$. After correcting for these d-wave resonances, we obtained a value for $\nu = 1.20^{+0.25}_{-0.28}$, which is also in agreement with the expected value of 1.0.

With the resolution and sensitivity of the present measurements, we obtained a complete sequence of the s-wave resonances up to $E_n \sim 250$ keV, almost a complete series of p-wave resonances and a certain fraction of d-wave resonances up to $E_n \sim 130$ keV.

D. Missing levels estimator

Another estimate for the correct number of resonances in a given level sequence can be made by the missing level estimator¹⁵ (M3) which uses properties of the Porter-Thomas law resulting from partial integration. The method consists of calculating the quantity $n\Sigma g\Gamma_n / (\Sigma \sqrt{g\Gamma_n})^2$ starting with the largest value of $g\Gamma_n$ in the interval and adding additional levels, one at a time, going from larger to smaller in the ordered array of observed values of $g\Gamma_n$. When this quantity equals 1.206, the total number of levels in the energy interval is assumed to be $n/0.617$. This method is quick and does not require any judgement except in respect to its sensitivity to the

TABLE V. Values of resonance parameters for all $\ell > 0$ resonances obtained up to 130 keV from a combination of total and capture cross section measurements. These are resonance energies E_0 , their uncertainties ΔE_0 , the capture area A_γ with uncertainties, $g\Gamma_n$, and the derived Γ_γ with their uncertainties. The last two columns give the assumed value of g and the calculated probability for a resonance to be d wave as explained in the text. For some resonances, $\Gamma_\gamma = 170$ meV was assumed to obtain $g\Gamma_n$ values.

E_0 (eV)	ΔE_0 (eV)	$A_\gamma = g\Gamma_\gamma\Gamma_n/\Gamma$ (meV)	S.D. (meV)	$g\Gamma_n$ (eV)	Γ_γ (meV)	Assumed g	P(d)
3801	3	56.0	1.2	0.084 ± 0.009	170	1	
7481	5	111.3	1.5	0.40 ± 0.04	77 ± 9	2	
8240	5	71.0	1.5	0.20 ± 0.02	110 ± 16	1	
8588	5	160.8	2.4	0.30 ± 0.03	173 ± 20	2	
9608	5	130.8	2.3	0.40 ± 0.04	194 ± 24	1	
12112	5	20.0	1.3	0.023 ± 0.002	170	1	
12899	5	2.0	0.8	0.002 ± 0.001	170	2	86
16015	5	193.6	4.8	1.70 ± 0.20	218 ± 30	1	
16126	5	18.5	1.7	0.021 ± 0.002	170	1	
18055	6	56.9	3.3	0.086 ± 0.009	170	1	
18400	6	158.8	4.6	1.30 ± 0.20	180 ± 22	1	
20230	6	138.2	5.2	0.33 ± 0.04	238 ± 30	2	
22843	7	81.6	3.1	0.80 ± 0.09	91 ± 10	1	
24741	7	271.9	8.8	1.25 ± 0.20	173 ± 20	2	
25907	7	42.4	4.1	0.06 ± 0.01	170	1	
26254	7	177.2	7.7	6.75 ± 0.40	178 ± 20	1	
27335	7	42.7	4.7	0.06 ± 0.01	170	1	
28543	8	200.2	9.2	3.50 ± 0.30	209 ± 30	1	
31928	8	78.4	7.4	0.15 ± 0.02	170	1	
32763	10	75.9	7.0	0.84 ± 0.10	82 ± 10	1	
33507	10	243.7	15.2	3.10 ± 0.30	130 ± 10	2	
34416	10	114.4	9.0	0.35 ± 0.04	170 ± 20	1	
36743	12	155.5	11.1	0.31 ± 0.03	156 ± 18	2	
36857	12	153.6	10.1	0.57 ± 0.06	210 ± 30	1	
37007	12	77.5	7.8	0.14 ± 0.02	170	1	
37886	12	87.9	7.7	0.59 ± 0.06	103 ± 15	1	
39270	12	178.7	11.6	9.50 ± 1.00	178 ± 20	1	
41792	12	60.4	7.9	0.09 ± 0.02	170	1	
44563	13	63.3	7.5	0.10 ± 0.02	170	1	
44815	13	84.1	7.5	0.17 ± 0.02	170	1	
45214	14	59.9	5.0	0.09 ± 0.02	170	1	
45760	14	103.5	7.4	0.30 ± 0.03	158 ± 18	1	
47870	14	29.7	12.8	0.04 ± 0.02	170	2	84
48026	14	94.3	21.2	0.21 ± 0.04	170	1	
48230	14	43.9	9.4	0.06 ± 0.02	170	2	69
50680	14	52.4	5.6	0.08 ± 0.01	170	2	59
50933	14	226.1	16.5	0.80 ± 0.10	158 ± 18	2	
53034	15	458.2	24.2	1.33 ± 0.12	350 ± 40	2	
53893	15	209.3	17.2	7.08 ± 0.50	213 ± 30	1	
55119	15	256.7	17.9	1.60 ± 0.20	153 ± 18	2	
55238	15	44.3	11.7	0.06 ± 0.01	170	2	82
55813	15	206.0	18.2	1.00 ± 0.10	130 ± 17	2	
56695	15	279.2	23.1	27.50 ± 1.70	132 ± 17	2	
57475	16	60.0	5.0	0.09 ± 0.02	170	2	70
59078	16	59.9	5.0	0.09 ± 0.02	170	2	73
61922	16	59.9	5.0	0.09 ± 0.02	170	2	77
62330	17	195.5	22.7	4.00 ± 0.45	205 ± 30	1	
62787	17	299.9	24.0	1.84 ± 0.20	179 ± 20	2	
63720	17	347.8	29.3	2.00 ± 0.20	211 ± 30	2	
64668	17	334.0	27.0	5.80 ± 0.50	176 ± 20	2	
67130	17	134.5	26.1	0.50 ± 0.10	184 ± 30	1	
68917	18	120.7	10.0	0.50 ± 0.10	159 ± 30	1	
69267	18	269.4	26.3	6.90 ± 0.80	139 ± 20	2	
70900	18	252.2	29.8	13.70 ± 1.00	126 ± 18	2	
74612	18	321.5	23.8	1.60 ± 0.20	201 ± 35	2	

TABLE V (continued)

E_0 (eV)	ΔE_0 (eV)	$A_\gamma = \frac{g\Gamma_\gamma\Gamma_n}{\Gamma}$ (meV)	S.D. (meV)	$g\Gamma_n$ (eV)	Γ_γ (meV)	Assumed g	P(d)
75087	18	245.9	21.6	0.58 ± 0.10	213 ± 35	2	
76380	18	202.1	19.5	2.50 ± 0.25	110 ± 18	2	
77104	18	419.5	28.5	2.00 ± 0.20	264 ± 35	2	
77418	18	225.4	22.6	3.20 ± 0.35	242 ± 35	1	
78331	19	87.4	8.0	0.18 ± 0.03	170	2	70
78600	19	59.9	5.0	0.04 ± 0.02	170	2	94
80759	19	297.3	29.1	24.60 ± 2.00	148 ± 22	2	
82300	19	284.3	26.4	2.20 ± 0.25	163 ± 25	2	
82784	19	103.2	9.0	0.30 ± 0.03	157 ± 25	1	
84460	19	48.5	15.2	0.07 ± 0.02	170	2	91
85670	19	171.7	20.3	3.50 ± 0.35	89 ± 20	2	
86690	19	93.2	9.0	2.30 ± 0.25	96 ± 20	1	
86960	19	94.7	9.0	5.90 ± 0.50	94 ± 20	1	
87000	19	386.5	79.9	45.00 ± 2.50	181 ± 40	2	
87290	19	94.3	0.8	5.70 ± 0.60	94 ± 10	1	
90225	20	90.0	36.5	0.19 ± 0.06	170	2	79
91161	20	140.0	19.2	0.24 ± 0.03	170	2	72
93380	20	108.3	33.1	0.35 ± 0.10	157 ± 40	2	53
93900	20	87.4	8.0	0.18 ± 0.02	170	2	83
94460	20	87.4	23.4	0.18 ± 0.03	170	2	83
94700	20	68.7	38.6	6.00 ± 0.60	68 ± 35	1	
96806	25	156.0	15.8	6.25 ± 0.60	157 ± 30	1	
97882	25	219.0	55.7	2.80 ± 0.30	237 ± 50	1	
99370	25	59.9	6.0	0.09 ± 0.01	170	2	90
99730	25	86.7	56.0	0.18 ± 0.10	170	2	85
101750	25	157.9	51.4	0.30 ± 0.10	170	2	72
102650	25	241.4	54.0	17.50 ± 1.50	116 ± 35	2	
102870	25	278.0	57.5	3.50 ± 0.35	150 ± 40	2	
104600	25	375.7	60.6	3.90 ± 0.35	207 ± 45	2	
106170	25	51.7	8.0	4.90 ± 0.45	50 ± 13	1	
108780 ^a	25	383.6	71.8	1.00 ± 0.20		2	
109210	25	149.0	15.0	21.00 ± 1.50	68 ± 11	2	
111610	30	153.0	15.0	13.10 ± 1.00	151 ± 23	1	
112380	30	276.4	60.0	1.80 ± 0.20	162 ± 45	2	
112660	30	267.4	60.4	1.80 ± 0.20	156 ± 45	2	
113420	30	255.0	64.8	33.40 ± 2.00	118 ± 30	2	
116920	30	98.3	73.6	1.00 ± 0.15	55 ± 40	2	
118540	30	101.7	73.5	93.40 ± 3.00	73 ± 50	1	
119450	30	138.2	25.0	0.23 ± 0.05	170	2	87
123095	30	105.1	51.9	5.00 ± 0.50	105 ± 50	1	
126670	30	361.0	80.5	4.60 ± 0.50	195 ± 50	2	
127320	30	206.6	60.5	4.60 ± 0.50	215 ± 70	1	
128550	30	150.9	66.4	6.30 ± 0.60	153 ± 45	1	
129340	30	188.3	70.0	2.20 ± 0.30	205 ± 80	1	
129750	30	97.6	62.2	3.60 ± 0.40	100 ± 55	1	

^aProbable doublet.

accuracies in the values of the largest widths, which can be determined with much greater accuracy than the smaller widths.

We have applied this analysis to the s-wave neutron widths up to 250 and 300 keV energy. We found that according to this estimate we lacked 1 neutron width up to 250 keV corresponding to about 2% loss of levels and perhaps a maximum of 3 neutron widths up to 300 keV. The prediction up to 250 keV was consistent with our investigation of the neutron width distribution, but we were unable to find additional s-wave resonances with significant asymmetrical shapes. This small discrepancy could be

due to a statistical fluctuation or to the sensitivity of the measurements and not necessarily to a deviation from the statistical theory. When we applied this technique (M3 estimator) to our observed p-wave level series, we found that 65 levels were predicted up to 130 keV, which was somewhat lower than that (80) obtained from the investigation of the p-wave neutron reduced width distribution.

E. Radiation widths (Γ_γ)

The capture cross section data provided areas ($g\Gamma_n\Gamma_\gamma/\Gamma$) under the resonances and

TABLE VI. The parameters (E_0 , ΔE_0 , $g\Gamma_n$) of $\ell > 0$ resonances obtained from the R-matrix analysis of the total cross section measurements.

E_0 (eV)	$g\Gamma_n$ (eV)						
131900 ± 30	3.4	188700 ± 30	5	254100 ± 50	76	323690 ± 55	70
136070 ± 30	3.4	189840 ± 30	26	257180 ± 50	73	324500 ± 55	45
136325 ± 15	3.8	190220 ± 30	9	258122 ± 50	40	327250 ± 55	45
137640 ± 15	3.1	191750 ± 30	6	258950 ± 50	40	329280 ± 50	15
140235 ± 15	13.0	191960 ± 30	59	262522 ± 50	28	330460 ± 50	05
140870 ± 15	4.0	200540 ± 35	14	262897 ± 50	129	332720 ± 50	46
141020 ± 15	4.0	205240 ± 35	24	263580 ± 50	34	335090 ± 50	39
143340 ± 15	8.1	208420 ± 35	39	267280 ± 50	91	340736 ± 50	14
146210 ± 15	33.0	210040 ± 35	43	270600 ± 50	83	342077 ± 50	62
149385 ± 15	6.4	211270 ± 35	15	272186 ± 50	64	343350 ± 50	58
150460 ± 20	7.0	213176 ± 35	11	272880 ± 50	62	346730 ± 50	12
151700 ± 20	5.5	213560 ± 35	142	274300 ± 50	19	347355 ± 50	10
153080 ± 20	8.4	213950 ± 35	17	275052 ± 50	150	350290 ± 50	20
154100 ± 20	10.5	219900 ± 35	36	276405 ± 50	125	353205 ± 50	54
155300 ± 20	30.0	223446 ± 40	23	281622 ± 50	113	353900 ± 50	83
158795 ± 20	10.2	224325 ± 40	23	286845 ± 50	400	355110 ± 50	60
159365 ± 20	60.0	225723 ± 40	32	292475 ± 50	253	356030 ± 50	52
163880 ± 20	20.0	227095 ± 40	53	293400 ± 50	63	358940 ± 50	47
166320 ± 25	5.8	227248 ± 40	30	296168 ± 50	79	364270 ± 60	88
167455 ± 25	5.3	229660 ± 40	14	298115 ± 50	120	367050 ± 60	92
168010 ± 25	1.9	230619 ± 40	14	299280 ± 50	204	367820 ± 60	54
168900 ± 25	5.3	231248 ± 40	12	301930 ± 55	38	370350 ± 60	24
172200 ± 25	7.8	231625 ± 40	5	303300 ± 55	10	371110 ± 60	53
173180 ± 25	10	233467 ± 40	37	304410 ± 55	22	373470 ± 60	55
177050 ± 25	3	234878 ± 40	32	306615 ± 55	45	375800 ± 60	31
177250 ± 30	100	235961 ± 40	17	308420 ± 55	70	376470 ± 60	38
178460 ± 30	20	239240 ± 40	89	311720 ± 55	52	377100 ± 60	10
179332 ± 30	8	240780 ± 40	28	316150 ± 55	105	380175 ± 60	12
182120 ± 30	40	244455 ± 40	48	316870 ± 55	53		
184060 ± 30	6	246050 ± 40	102	317230 ± 55	46		
186370 ± 30	15	252080 ± 50	37	318245 ± 55	28		

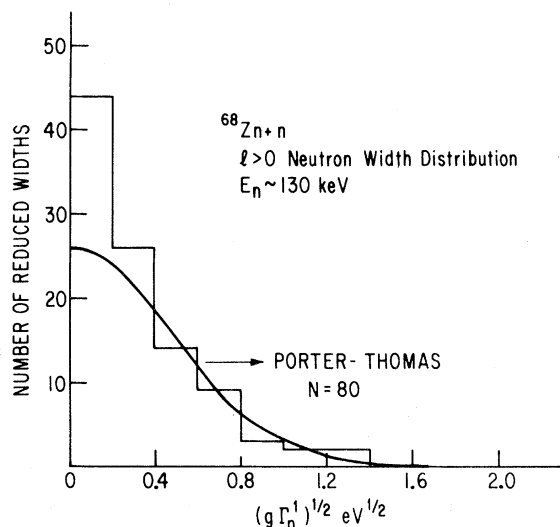


FIG. 8. The histogram plot of the neutron reduced width amplitude distribution for 80 p-wave resonances after elimination of d-wave resonances. The solid curve is the theoretical Porter-Thomas distribution for a single sequence.

using values of $g\Gamma_n$ from transmission data, values of Γ_γ for s-wave resonances were obtained. These values of Γ_γ had to be corrected for the scattered neutron sensitivity factor, k . The values of k for ^{68}Zn have been determined by using a procedure published by Allen et al.¹⁶ These values of k , as well as resonance capture area, A , Γ_n and corrected Γ_γ , are given in Table III up to $E_n \sim 125$ keV.

The values of Γ_γ for individual resonances showed a wide variation, in contrast to data on many heavy nuclei. From these we obtained a mean value of $(\Gamma_\gamma)_{\ell=0} = (302 \pm 60)$ meV where the uncertainty is obtained from the relation S/\sqrt{n} , where S is the standard deviation of a normal distribution and n is the number of widths measured.

F. $\ell > 0$ radiation widths

We obtained $g\Gamma_\gamma$ for many $\ell > 0$ resonances from capture areas and values of $g\Gamma_n$ from the transmission data. If g is also known, values of Γ_γ can be obtained. However, as mentioned earlier a large number of resonances was observed only in the capture measurements. The $g\Gamma_n$ values of these resonances are in general much smaller or at most comparable to Γ_γ (Table V). In

such cases it was possible, by means of the LSFIT program,¹⁴ to determine $g\Gamma_n$ values for an assumed value of Γ_γ . If $\Gamma_\gamma \gg g\Gamma_n$, the capture area is almost equal to $g\Gamma_n$ and is quite insensitive to the assumed value of Γ_γ . However, if Γ_γ is comparable, the $g\Gamma_n$ values will depend on the assumed value of Γ_γ . For our analysis of $^{68}\text{Zn}+n$ data, we assumed a value of $\Gamma_\gamma = 170$ meV similar to the case $^{66}\text{Zn}+n$.⁶ We have also obtained a large number of Γ_γ values from the capture data for measured values of $g\Gamma_n$ and assumed value of g . From these we obtained the mean value of the radiation width $\langle \Gamma_\gamma \rangle_{\ell>0} = (157 \pm 7)$ meV, which is slightly lower than the assumed value of 170 meV. If the smaller Γ_γ values had been used, the $g\Gamma_n$ values would have been larger. We found that for 36 resonances, where $\Gamma_\gamma = 170$ meV was assumed, the change in $g\Gamma_n$ by using a lower value of Γ_γ of 150 meV varied from 1/2% to the worst case of 20% with the majority of the values between 2% and 4%. Hence, the difference in assumed value of Γ_γ would not significantly alter any of the conclusions about S_1 . Twenty of the narrowest widths have probabilities greater than 50% to be d wave and the effect of chosen Γ_γ value on d wave strength functions could be significant, as will be discussed in a later section.

An examination of Table II indicates that for s-wave resonances, individual Γ_γ values fluctuate widely about the mean value; whereas, for $\ell>0$ resonances (Table V), the individual radiation widths fluctuate less about their mean. These distributions can be represented by a chi-squared distribution with approximately as many degrees of freedom (ν) as there are primary transitions. The usual distribution for such a sum of transitions can be given as a chi-squared distribution with ν degrees of freedom and

$$\frac{2}{\nu} = [\langle \Gamma_{\gamma i}^2 \rangle - \langle \Gamma_{\gamma i} \rangle^2] / \langle \Gamma_{\gamma i} \rangle^2,$$

which represents the fractional mean squared spread in the $\Gamma_{\gamma i}$ values. From an analysis of the data using the above expression, we obtained a value for $\nu=20$ for $\ell>0$ radiation widths and 2.2 for s wave resonances. These results indicate that for s wave resonances, Γ_γ is dominated by only a few transitions to low lying negative parity states, whereas for p wave resonances Γ_γ is the sum of about twenty transitions to higher lying positive parity states. This effect would explain to some degree the relatively smaller value of $\langle \Gamma_\gamma \rangle_{\ell>0}$ compared to $\langle \Gamma_\gamma \rangle_{\ell=0}$, since the transitions for p-wave levels should involve low energy transitions and thus lower strengths. Most probably the major difference in Γ_γ values for s and p wave arises due to external or direct capture.

G. Level density

The level density¹⁷ based on the Fermi gas model can be given as a function of J at a given energy of excitation as

$$\rho_J(U) = \rho_0(U)(2J+1)\exp\left[\frac{-(J+1/2)^2}{2\sigma^2}\right].$$

Here σ is the cutoff parameter and is related to the moment of inertia of the nucleus. For the ^{68}Zn nucleus the capture of s-wave neutrons gives rise to excited states of unique $J^\pi = 1/2^+$; whereas, the capture of p-wave neutrons populates resonances with $J^\pi = 1/2^-$ and $3/2^-$.

The values of the average level spacing $D_{\ell=0}$ for s-wave resonances for different energy intervals are given in Table VII; we have chosen the value (5.56 ± 0.43) keV up to 250 keV as a final value. Similarly, the mean spacing for p-wave resonances up to 130 keV has been obtained from 80 resonances after eliminating the d-wave resonances. This gave a value for $D_1 = (1.63 \pm 0.14)$ keV. Using the above formula and a value of $\sigma^2 = 10$ from Baba,¹⁸ we obtained a ratio of level density $\rho_{\ell=1}/\rho_{\ell=0} = 2.69$ compared to the experimental value of this ratio of $(3.41^{+0.61}_{-0.51})$, indicating an excess of p-wave resonances. A similar calculation for the ratio of d-wave to s-wave resonances would give a ratio of $\rho_{\ell=2}/\rho_{\ell=0} = 3.73$ giving the value of d-wave mean spacing of $D_2 = 1.49$ keV. Thus, one should have observed about 87 d-wave resonances up to $E_n \sim 130$ keV. Based on Bayes theorem,¹⁹ we assigned only 20 resonances up to this energy, only $\sim 23\%$ of the expected number.

H. Level spacing distribution

The simplest possible case for the investigation of level energies of complex states was discussed by Wigner in terms of an interaction Hamiltonian consisting of 2×2 matrices belonging to an ensemble of matrices called the Gaussian orthogonal ensemble or, in short, GOE. Using these arguments, Wigner¹ surmised an expression for the joint probability distribution of nearest neighbor spacings (S) of levels of the same J^π as

$$P(x)dx = (\pi/2) x e^{-\frac{\pi x^2}{4}}, \text{ where } x = S/D.$$

This expression, though not mathematically exact in the limit $n \rightarrow \infty$, where n is the

TABLE VII. The number of resonances, the calculated mean level spacing, Δ_3 values (calculated and theoretical), nearest neighbor spacing correlation for the s-wave resonances observed in various energy intervals.

E_n (keV)	No. of levels	D (keV)	Δ_3 experi- mental	Δ_3 Theo- retical	ρ (corre- lation coeffi- cient)
0-100	18	5.56 ± 0.68	0.22	0.29	-0.13
0-200	36	5.56 ± 0.48	0.28	0.36	-0.27
0-250	45	5.56 ± 0.43	0.38	0.38	-0.24
0-300	56	5.38 ± 0.37	0.87	0.40	-0.22

dimensionality of the matrix ensemble, is indeed close and can not be distinguished experimentally from the exact result obtained by Mehta and Gaudin.²⁰ Even though these results are valid for the central region of the semicircle where the level density is constant, Monte Carlo calculations have, however, shown that within statistical sampling errors, the distributions are independent of the energy range chosen and coincide with the result of Mehta and Gaudin.²⁰

A plot of the experimental nearest neighbor level spacing distribution for $^{68}\text{Zn}+n$ up to $E_n \sim 250$ keV is shown in Fig. 9. This shows an excellent agreement with the Wigner distribution over the entire range. The data, for reasons of statistics, have been plotted as histograms for intervals of $\Delta x = 0.4$, where $x = S/D$. For a mean s-wave level spacing of 5.56 keV observed in these experiments, this interval is 2.2 keV compared to the energy resolution of about 0.35 keV at the maximum energy of 250 keV. The Wigner distribution predicts zero probability for $x = 0$, i.e., a level repulsion effect. With our present resolution, it was possible to resolve levels which were separated by about 0.2 keV at about 200 keV and much closer at lower energies. At 200 keV this corresponds to a value of x of ~ 0.04 . The probability for this spacing to occur for a Wigner distribution is 1%, or at most one level out of a total of 50 spacings; we did not observe any such small spacings. If the levels were to occur randomly due to random configuration mixing, one would expect about 4 such small spacings in this interval from 0 to 0.04.

In summary, the present data confirms without doubt the validity of GOE for the distribution of level energies of given J^π at high excitation energies. This level repulsion effect also implies that there is a negative short range correlation between nearest neighbor spacings. The magnitude of this correlation has been predicted by Porter²¹ to be -0.253 for a large number of resonances. Our calculation of this quantity up to 250 keV gave a value of -0.24 in excellent agreement with this prediction. The experimental value up to 300 keV decreased slightly to -0.22 , which may likely be due to some impurity in the level sequence in the 200-300 keV energy interval.

Considerable attention has been given in the past decade to the presence of a long range correlation between the level energies (the Δ_3 statistic) discussed by Dyson and Mehta.³ This quantity is defined as

$$\Delta_3 = 1/\pi^2 (\lambda_n n - 0.0687),$$

with a standard deviation of about 0.11 irrespective of the number of levels in the series. For an impure sequence of levels, this statistic was shown to deviate erratically showing no particular trend in view of the compensating nature of level occurrence according to a staircase plot of the number of levels vs E_n .

Some earlier investigations of this sta-

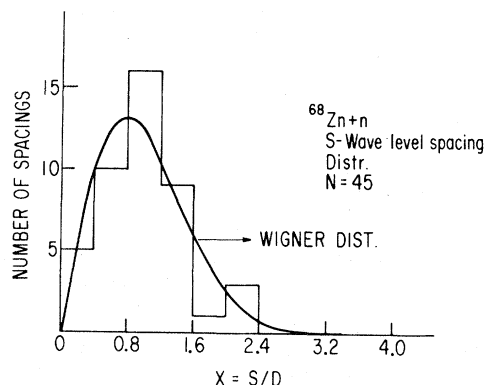


FIG. 9. The distribution of the nearest neighbor spacings of 45 s-wave resonances observed up to $E_n \sim 250$ keV. The solid curve is the Wigner distribution.

tistically by Liou et al.,⁴ the isotopes of erbium gave surprisingly good agreement with the theory and have generated interest to investigate its validity more carefully using data with less ambiguity. However, it was obvious from our high-resolution measurements^{5,6} on the even-even nuclides ^{64}Zn and ^{66}Zn , that even those data could not be completely relied on to prove the validity of the Δ_3 statistic in view of the great sensitivity of Δ_3 to the precise location of a single level in a series of the same J^π .

We have observed experimentally that the strategic location of a single level can sometimes drastically change the value of Δ_3 . This usually occurs if there is a large gap between two consecutive level energies. The calculated values of Δ_3 obtained from these experiments are given in Table VII. It can be seen that the experimental value of Δ_3 of 0.38 for 45 s-wave resonances up to $E_n \sim 250$ keV is in excellent agreement with the Dyson-Mehta theoretical value of 0.38. The results for smaller energy intervals, though smaller than the theoretical value, agree within the expected uncertainty of ± 0.11 . However, the experimental value of Δ_3 above 350 keV increases gradually until it gives a much larger value of 0.87 up to $E_n \sim 300$ keV, compared to a theoretical value of 0.40. It was, however, possible to obtain a value in agreement with the theoretical value, if one or two weak resonances were eliminated from this s-wave sequence. For example, if we eliminated the resonances at ~ 185 keV ($\Gamma_n \sim 30$ eV) and 270 keV ($\Gamma_n = 80$ eV) in Table IV from the s-wave series, we obtained a value of 0.48, in good agreement with the theoretical value. Similarly, if the resonance at 251.3 keV was deleted from the s-wave level sequence, we obtained a value of 0.56. However, these resonances are definitely s wave due to their asymmetric shapes. The addition of weak resonances beyond 250 keV did not produce agreement with the theory. We conclude that our data for 45 s-wave resonances up to 250 keV are in good agreement with the

Δ_3 statistic, but the comparison above this energy is not meaningful.

I. Strength functions

The giant resonance behavior of neutron strengths as a function of mass number has been successfully explained by the optical model.²² The location and widths of these resonances for s-, p- and d-wave neutron scattering depends upon the parameters of the optical potential. The average strength function for a given ℓ over the energy region ΔE is

$$S_\ell = \frac{\sum g_J \Gamma_n^\ell}{(2\ell + 1) \Delta E},$$

where ℓ and J refer to the angular momentum of the neutron and the total spin of the compound state, respectively.

The cumulative sum of $\Sigma \Gamma_n^0$ for s-wave resonances as a function of neutron energy is plotted in Fig. 10. The s-wave strength function for the entire interval is the slope of the straight line passing through the experimental points. However, because of the random statistical distribution of widths and effects, such as intermediate structure, the data points do not lie on one straight line. The three straight lines in Fig. 10 give different values of the strength function for different energy intervals. This variation is suggestive of possible doorway states.²³

A summary of the strength function values in increasing intervals of neutron energy is given in Table VIII. The value for the entire interval is $(2.01 \pm 0.34) \times 10^{-4}$. It is obvious that the uncertainty in the value decreases as the number of levels included in the analysis increases. The method for the determination of this uncertainty has been discussed by several authors.^{24, 25}

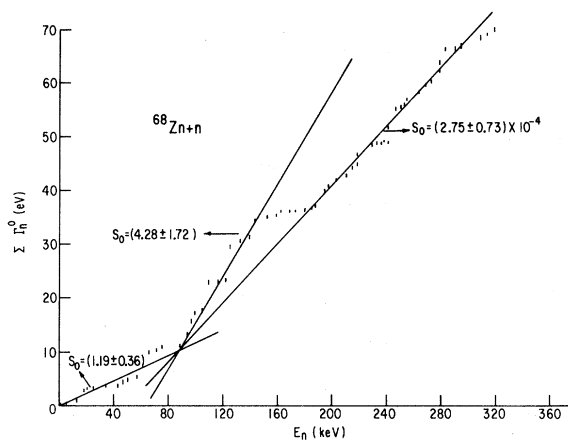


FIG. 10. A cumulative plot of the sum of the s-wave neutron reduced widths as a function of neutron energy. The solid curves are drawn through all the points in a given energy interval. The slopes of these straight lines can provide the values of s-wave strength function.

TABLE VIII. s- and p-wave neutron strength function values obtained from different energy intervals of neutron energy. A value of the nuclear radius $R = 5.6$ fm was used for the calculation of p-wave neutron reduced widths.

E_n (keV)	S_0 in units of 10^{-4}	S_1 in units of 10^{-4}
0-100	1.70 ± 0.56	0.49 ± 0.08
0-130	2.07 ± 0.48	0.49 ± 0.07
0-200	2.07 ± 0.48	0.47 ± 0.05
0-300	2.28 ± 0.43	0.56 ± 0.05
0-380	2.01 ± 0.34	0.60 ± 0.05
100-200	2.38 ± 0.78	0.42 ± 0.06
200-300	2.63 ± 0.89	0.75 ± 0.10
300-380	1.16 ± 0.38	0.84 ± 0.15

A similar cumulative plot of $\Sigma g \Gamma_n^1$ vs E_n is shown in Fig. 11. Here also we see that not all the data points pass through a smooth straight line. The values of S_1 for different energy intervals are given in Table VIII. We chose the final value of $S_1 = (0.56 \pm 0.05) \times 10^{-4}$ up to 300 keV, since we felt less certain of the accurate determination of p-wave widths above this energy due to resolution effects. We found $S_1 = (0.49 \pm 0.07)$ up to $E_n \sim 130$ keV, where both transmission and capture data were included. The sharp increase in S_1 at about $E_n \sim 260$ keV in Fig. 11, up to the maximum energy of $E_n \sim 380$ keV, may also be due to the presence of a doorway state.

J. d-wave strength function

A value of the d-wave strength function S_2 of $(0.13 \pm 0.03) \times 10^{-4}$ was obtained from the 20 assigned d-wave resonances. The uncertainty is purely statistical in nature. From a comparison of the d-wave neutron reduced width distribution with the Porter-Thomas distribution, we obtained a

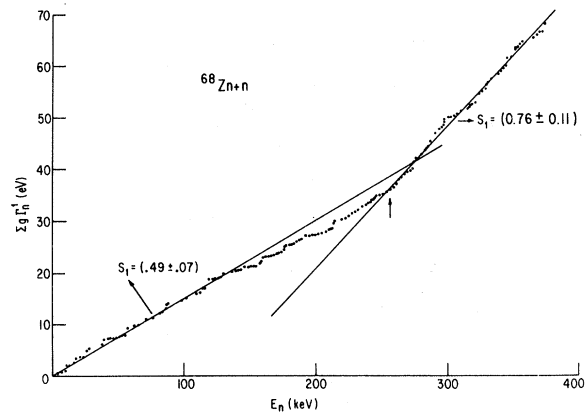


FIG. 11. A cumulative plot of the sum of the p-wave neutron reduced widths as a function of neutron energy. The solid curves are drawn through the points.

correction of about 50% in S_2 from the missed weak levels. This gave a corrected value of S_2 of (0.20 ± 0.06) . However, because of the uncertainties of the spins and Γ_γ 's of these d-wave resonances the uncertainty was increased to ± 0.10 .

K. Correlation between Γ_n^0 and Γ_γ for s-wave resonances

As mentioned earlier we have determined the radiation widths of about 22 s-wave resonances up to 130 keV from the measurement of the capture areas. A large positive correlation of 0.5 between Γ_n and Γ_γ ($P > 99.7\%$) was found for these 22 resonances. Similar strong correlations have been previously observed for other even-even nuclides such as $^{64}\text{Zn}+n$ and $^{66}\text{Zn}+n$ reactions.^{5,6} These observations show that nonstatistical effects must be present for these nuclides.

L. Average capture cross section

We have calculated the average capture cross section in neutron energy intervals of 5, 10 and 20 keV. These are shown in Table IX. These cross sections fluctuate rapidly at lower energies because of the presence of well resolved resonances; however, the average cross section varies smoothly above about 30 keV. These cross sections have been corrected by the factor 0.95 for an error in the normalization procedure used during the data processing.²⁶ The average value of 19.2 mb was obtained at $E_n \sim (30 \pm 10)$ keV. This quantity is of interest for nucleosynthesis of elements in stars.

M. Thermal energy neutron data

The coherent and bound neutron scattering cross sections of ^{68}Zn as well as the capture cross section at thermal neutron energy have been measured and recommended values published.⁸ It is interesting to compute values of these cross sections from the measured resonance parameters of the present experiment. It is found that almost all the contributions to these cross sections arise from the s-wave resonance at 516.4 eV and from the value of $R = 5.6$ fm. We have fitted the total cross section data observed in the present measurement from a few eV to about 20 keV using an R-matrix code²⁷ and have computed thermal values of $\sigma_s = 5.78$ b, $\sigma_{\text{coh}} = 5.89$ b, and $\sigma_{n\gamma} \sim 1.0$ b which are in excellent agreement with the measured values. Hence, the thermal data do not warrant the presence of a bound level near the thermal neutron energy. For the capture cross section, a value of Γ_γ of 0.167 eV was assumed. This analysis also provided a value of effective nuclear radius (R') of 5.85 fm which was obtained from the expression $R' = (1-A_j)R$.

TABLE IX. The average capture cross section as a function of neutron energy interval. The data have been corrected for the normalization error (Ref. 26) of 0.95.

E_n (keV)	$\sigma_{n\gamma}$ (mb)	E_n (keV)	$\sigma_{n\gamma}$ (mb)
3-9	117.1	220-240	11.2
9-15	43.3	240-260	11.2
15-20	40.7	260-280	10.8
20-30	20.2	280-300	12.6
30-40	18.3	300-320	9.9
40-50	17.1	320-340	11.0
50-60	21.4	340-360	11.6
60-80	20.2	360-380	11.3
80-100	12.6	380-400	11.9
100-200	13.3	400-420	10.1
120-140	13.9	420-440	11.6
140-160	14.6	440-460	14.8
160-180	12.8	460-480	12.7
180-200	12.1	480-500	13.0
200-220	11.4		

V. SUMMARY

The distribution of the statistical properties, such as reduced neutron widths and level spacings for s-wave resonances obtained from high-resolution transmission and capture measurements on ^{68}Zn , were in excellent agreement with the Porter-Thomas and Wigner distributions and with the Δ_3 statistic of Dyson and Mehta. The validity of this Δ_3 statistic permits one to predict the mean level spacing more precisely than would be the case if the levels were randomly distributed or showed no long range correlations. Average quantities, such as the mean level spacings, radiation widths and strength functions for both s- and p-wave neutrons were obtained. The variation of the strength functions with energy is suggestive of possible doorway states.

The significant correlation between neutron and radiation widths is evidence of a nonstatistical process. The wide spread in radiation widths obtained for s-wave resonances probably occurs because of a few strong transitions to low-lying negative parity states.

This research was sponsored by the Division of Nuclear Sciences, U.S. Department of Energy, under Contract No. W-7405-eng-26 with the Union Carbide Corporation and Contract No. DE-AC02-76ER02439 with the State University of New York at Albany. One of us (V.K.T.) would like to express his gratitude to the Saha Institute of Nuclear Physics for a leave of absence.

- ¹E.P. Wigner, Proceedings of the Gatlinburg Conference on Neutron Time-of-Flight Methods, Oak Ridge National Laboratory Report ORNL-2309, 1957.
- ²C.E. Porter and R.G. Thomas, Phys. Rev. 104, 483 (1956).
- ³F.J. Dyson, J. Math. Phys. 3, 140 (1962); 3, 157 (1962); 3, 166 (1962); 3, 1199 (1962); F.J. Dyson and M.L. Mehta, *ibid.* 4, 701 (1963).
- ⁴H.I. Liou, H.S. Camarda, S. Wynchank, M. Slagowitz, G. Hacken, F. Rahn, and J. Rainwater, Phys. Rev. C 5, 974 (1972).
- ⁵J.B. Garg, V.K. Tikku, and J.A. Harvey, Phys. Rev. C 23, 671 (1980); J.B. Garg, V.K. Tikku, R.L. Macklin, and J. Halperin, *ibid.* (in press).
- ⁶J.B. Garg, V.K. Tikku, J.A. Harvey, R.L. Macklin, and J. Halperin, Phys. Rev. C (in press).
- ⁷E. P. Wigner and L. Eisenbud, Phys. Rev. 72, 29 (1947).
- ⁸Neutron Cross Sections, Vol. I, Resonance Parameters, edited by S.F. Mughabghab and D.F. Garber, Brookhaven National Laboratory Report BNL-325, 3rd edition, 1973.
- ⁹C.A. Barnes, in Nucleosynthesis and Neutron Capture Cross Sections in Advances in Nuclear Physics, edited by M. Baranger and Erich Vogt (Plenum, New York, 1971), Vol. 4.
- ¹⁰M.S. Pandey, J.B. Garg, and J.A. Harvey, Phys. Rev. C 15, 600 (1977).
- ¹¹R.L. Macklin and B.J. Allen, Nucl. Instrum. Methods 91, 565 (1971).
- ¹²J.B. Garg, S. Jain, and J.A. Harvey, Phys. Rev. C 18, 1141 (1978).
- ¹³G.F. Auchampaugh, code MULTI, Los Alamos National Laboratory Report LA-5473-MS, 1974.
- ¹⁴R.L. Macklin, Nucl. Instrum. Methods 91, 79 (1971).
- ¹⁵M.S. Moore, J.D. Moses, G.A. Keyworth, J.W.T. Dabbs, and N.W. Hill, Phys. Rev. C 18, 1328 (1978).
- ¹⁶B.J. Allen, R.L. Macklin, R.R. Winters, and C.Y. Fu, Phys. Rev. C 8, 1504 (1973).
- ¹⁷C. Bloch, Proceedings of International Conference on Statistical Properties of Nuclei, edited by J.B. Garg (Plenum, New York, 1972), p. 379.
- ¹⁸H. Baba, Nucl. Phys. A159, No. 2, 625 (1970).
- ¹⁹H. Cramer, The Elements of Probability Theory (Wiley, New York, 1954).
- ²⁰M.L. Mehta, Nucl. Phys. 18, 395 (1960); M. Gaudin, *ibid.* 25, 447 (1961).
- ²¹C.E. Porter, Nucl. Phys. 40, 167 (1963).
- ²²C.E. Porter, H. Feshbach, and V.F. Weisskopf, Phys. Rev. 96, 448 (1954).
- ²³B. Bloch and H. Feshbach, Ann. Phys. (N.Y.) 23, 47 (1963).
- ²⁴H.I. Liou and J. Rainwater, Phys. Rev. C 6, 435 (1972); H.V. Muradyan and Y.V. Adamchuk, Nucl. Phys. 68, 549 (1966); D.V. Slavinskis and T.J. Kennett, *ibid.* 85, 641 (1966).
- ²⁵J.B. Garg, J. Rainwater, J.S. Petersen, and W.W. Havens, Jr., Phys. Rev. 134, B985 (1964).
- ²⁶R.L. Macklin and R.R. Winters, Nucl. Sci. Eng. 78, 110 (1981).
- ²⁷J.B. Garg, J. Rainwater, and W.W. Havens, Jr., Phys. Rev. C 3, 2447 (1971).